Geospatial Health
Geospatial Health 2026; 21:1409
doi:10.4081/gh.2026.1409

Reduction of latency in geospatial analysis of air quality: a classical modelling approach inspired by quantum principles

Hooshang Eivazy

Geoscience Department, Arak University of Technology, Arak, Iran

Abstract

Inspired by conceptual principles from quantum information theory, a novel classical approach to address temporal delays in spatial data analysis is presented. Current geospatial services face latency challenges due to complex processing chains, which motivate an investigation of whether the quantum-inspired paradigm could offer efficiency gains when implemented using classical hardware. A framework is proposed that incorporates three metaphors derived from quantum concepts: i) application of bit-like representation that mimics Qubit superposition to handle data uncertainty probabilistically; ii) use of probabilistic distributions for handling data uncertainty; and iii) creation of efficient data linkages by establishing pre-computed spatial correlations as an analogue to quantum entanglement. This model suggests potential temporal improvements while acknowledging current classical computing limitations. The proof-of-concept was tested on urban air quality monitoring, integrating data from fixed stations and mobile sensors. Simulation results indicated potential latency reduction while maintaining analytical accuracy (mean error <5.2% in controlled tests). Compared to the standard classical methods, the quantum-inspired metaphor showed efficiency improvements in theory when scaled to appropriate problem sizes, with simulated refresh rates of 250 milliseconds. Error analysis support the usefulness of the system for environmental health applications running on existing classical infrastructure. This research contributes: i) a framework for using quantum-inspired metaphors to address temporal challenges in geospatial analysis; ii) a simulation prototype for air quality monitoring; and iii) preliminary evidence of potential advantages from a bio-inspired approach in GIS processing. The technique may prove valuable for time-sensitive applications with today's technology and could inform future designs for potential quantum computing implementations.

Key words: classical approach inspired by quantum concepts, air quality information services, GIS.

Correspondence: Hooshang Eivazy, Geoscience Department, Arak University of Technology, Arak, Iran. Tel.: +98.9371985758.
E-mail: h.eivazy@arakut.ac.ir

Introduction

During the past decade, Geographical Information Systems (GIS) have mostly included initial processing of spatial data processing achieveable by executing one or two spatial functions. The implementation and execution of web-based services for this type of processing have become increasingly feasible and accessible through modern GeoAI frameworks (Janowicz *et al.*, 2020). Currently, however, the use of GIS has become much more complex, including demands that can only be met through the design and implementation of a chain of relatively intricate spatial functions. Such chains often rely on advanced machine learning techniques that require specialized expertise in spatial analysis (Goel *et al.*, 2023). Since the execution of such chains is time-consuming and costly (depending if they require data monthly, daily or every few hours), this type of real-time processing cannot easily be performed. Online access to such services is also questionable since an information map may be shared online through a web service, while the information provided is not always up-to-date. Presently, only information with relatively simple contents can reach this level of accuracy. For example, the traffic speed on Google Maps is solely displayed based on the speedometer as observed by users. Another problem is the lack of required reference points that can be problematic in cases with limited input, *e.g.*, in the relatively large city of Arak City in Markazi Province, Iran where there are only three permanent stations for air quality monitoring and control. Even if all three work properly, interpolation of urban air quality over an area of more than 100 km^2 cannot be accurate. As a solution, this article proposes a quantum-inspired framework addressing the challenges in real-time spatial data processing.

Regarding the problem of the lack of reference points, the most logical way would be to increase the number of air quality monitoring stations. However, this has traditionally been impractical due to the high price of required equipment. Recent developments in low-cost sensing technologies offer a promising alternative (Omidvar *et al.*, 2021). Another solution would be to use methods based on crowdsourcing or Volunteered Geographic Information (VGI); *e.g.*, vehicle speed and tracking data can be extracted from traffic videos to estimate road conditions (Hua *et al.* , 2018). However, information on air-quality parameters cannot be measured with ordinary smartphone sensors and remains therefore expensive and inaccessible for the public use. Consequently, col-

lecting such data cannot realistically rely on common VGI or crowd-sourcing approaches, which typically depend on widespread user participation with low-cost tools. This limitation aligns with broader findings in the literature showing that crowd-sourcing often fails when the required contributions demand specialized equipment, expertise or high-effort participation (Dahlander & Piezunka, 2020). Although satellite imagery has been widely used in air-quality monitoring, such data generally lack the temporal resolution required for real-time or near-real-time applications. Satellite-derived Aerosol Optical Depth (AOD), as used by Zheng *et al.* (2016), provides valuable large-scale estimates of surface-level particulate matter with a diameter of $\leq$2.5 µm ($PM_{2.5}$), but the acquisition frequency is limited and does not support continuous, on-demand monitoring. Therefore, relying solely on satellite observations is not suitable for applications that require timely and successive air-quality information. In addition, air quality pollutant parameters cannot be expected to be extracted from these images with any degree of accuracy.

Rather than relying solely on accessible online data sources, the computational load and time required for data preparation present significant challenges. To mitigate these processing demands, automated workflows and scalable solutions are essential. Implementing custom programming, leveraging adaptable GIS platforms, and utilizing intelligent processing agents represent viable approaches for streamlining these tasks (Mete & Yomralioglu, 2021). However, these methods cannot be relied on for performing complex spatial analysis. Artificial Intelligence (AI), on the other hand, can extract data, perform calculations and provide results regularly (*e.g.*, every hour). However, this would require an Application Programming Interface (API) allowing connection to an AI-capable webpage, automatic data retrieval and processing. Essentially, it involves setting up an API to fetch data from the webpage, using it to feed the data for processing, automating and establishment of a schedule (*e.g.*, using a scheduler) and finally displaying the results on a webpage or through another interface. This approach, while capable of data processing, still faces limitations in performing complex spatial analysis that requires a deeper understanding of spatial relationships.

AI has so far not been integrated with the complex spatial analyses as those carried out by ArcGIS (ESRI, Redlands, CA, USA) or other similar programmes. For example, ArcGIS Pro has specialized tools and complex algorithms designed for analyzing spatial data that are limited to searching and extracting geographic information, carrying out simple spatial calculations and utilizing simple statistical analysis. While AI, deep learning, and machine learning are increasingly applied to image processing tasks in various scientific fields (Ali *et al.*, 2025), these applications do not yet match the integrated and complex spatial analysis functionalities of dedicated geospatial software. One of the best approaches would be to use specialized automated spatial process builders, such as the Model Builder function developed by ESRI (Shaharudin *et al.*, 2025). However, depending on their complexity and the volume of data being processed, executing these models can sometimes take several hours. On the other hand, it is not always possible to execute the entire processing chain using a single model since part of the spatial processing chain must be performed through human agents in certain situations and the analytical intelligence of spatial analysts, a process that can take hours. These issues make the online and real-time execution of some complex spatial chains impossible. Companies such as Foursquare (https://foursquare.com/), a leading location-intelligence platform, apply a similar approach by simulating spatial processes through Structured Query Language (SQL) functions and basic mathematical formulations, as demonstrated by Ilba (2025). This method allows rapidly performing a large number of queries on a relatively large dataset. However, executing a chain of complex functions is not possible through this method.

The reviewed approaches collectively highlight a fundamental tensor (a mathematical object generalizing scalar, vector and linear operations) in spatial data analysis representing a trade-off between computational cost, temporal latency and analytical complexity. While solutions exist for automating individual steps, a paradigm capable of delivering near-real-time results for complex spatial chains without massive infrastructure investment remains elusive. Instead of seeking incremental optimization within the classical sequential processing paradigm, this paper explores whether quantum-inspired metaphors–specifically, probabilistic bit-like representation, probabilistic distributions and pre-computed spatial correlations emulating entanglement–can be emulated on classical hardware to create a more efficient framework. The approach does not claim to outperform dedicated high-performance computing in all aspects but rather investigate a novel bio-inspired pathway to rethink spatial data linkage and processing. The primary contribution is a proof-of-concept that demonstrates the potential of this paradigm for applications like urban air quality monitoring, where timeliness is critical, thus offering a new perspective on a persistent problem in the field.

Quantum computing

The potential applications of quantum computing are vast – from cracking modern encryption methods to revolutionizing drug discovery, materials science, artificial intelligence, Remote Sensing (RS) (Miroszewski*et al.* , 2023) and GIS (Werner, 2019). Despite these exciting possibilities, significant challenges remain, such as the need for ultra-cold operating temperatures and the difficulty of scaling up systems to handle real-world problems. While still in its early stages, quantum computing holds the promise of transforming technology in ways we are just beginning to imagine. This work is conceptually inspired by two fundamental principles of quantum information theory – superposition and entanglement – to address latency in classical spatial data processing. These principles are adapted as metaphorical frameworks rather than physical implementations, tailoring them for efficient computation on classical hardware. The first metaphor leverages the concept of superposition: unlike a deterministic classical bit, a quantum computing Qubit can exist in a probabilistic mixture of states |0> and |1> (Memon *et al.* , 2024). This is translated to a probabilistic data representation for handling uncertainty in spatial measurements (*e.g.*, from mobile sensors). Instead of a single, deterministic value, a data point can be represented by a probability distribution, allowing the system to process a spectrum of possible states simultaneously in a computational model. The second metaphor utilizes the concept of entanglement that describes strong correlations where the state of one Qubit instantly influences the other. In our classical model, this inspires the pre-computation and storage of spatial correlation matrices. For a given spatial domain (*e.g.*, an urban area), the statistical correlations between different locations are pre-computed. In this way, pre-established linkages become analogous to «classical entanglement,» allowing for near-instantaneous data updates across the network once a new measurement is included, significantly reducing the latency of recalculating correlations 'on-the-fly'. By combining these two metaphors, the model can achieve a more efficient handling of uncertain, dynamic spatial data streams, mimicking the parallel processing and strong correlation advantages of quantum systems within a classical computing paradigm.

Materials and Methods

While not an implementation on actual quantum hardware, this work explores how quantum computing principles could theoretically enhance geospatial analysis. The study focuses on air quality monitoring in Arak City as a proof-of-concept case study. The solution proposed and the formalism employed consists of using classically emulated quantum principles for spatial processing, which requires some mathematical formula, *i.e.* this paper utilizes the Dirac notation ($|\psi\rangle$ to describe the state of the spatial system. This choice is motivated by the fact that the algorithmic architecture and its core logic – particularly the treatment of non-local spatial dependence as a form of «entanglement-inspired correlation» – are directly inspired by quantum theory principles (Lin, 2022). It is crucial to distinguish this conceptual inspiration from physical implementation: all computations are performed on classical hardware using high-performance classical computing paradigms based on the use of Graphic Processors Units (GPUs). The quantum-inspired notation serves as a unifying and intuitive mathematical framework for representing complex spatial probability distributions and their interactions, highlighting the novel theoretical basis of our approach without claiming quantum physical execution.

The proposed framework exhibits a form of Qubit-inspired data representation. While quantum systems leverage Qubit superposition (simultaneous 0 and 1 states), the classical implementation models this probabilistically, with each pixel's value representing a probability distribution: $|P\rangle = \alpha|0\rangle + \beta|1\rangle$ where $|0\rangle$, $|1\rangle$ are the basis states (*e.g.*, «correct»/»incorrect» classifications) and α and β are the classical probability amplitudes ($|\alpha|^2 + |\beta|^2 =$ quantum superpositions without requiring physical Qubits, operating entirely on classical hardware. Quantum entanglement is simulated through spatial dependency matrices whose pixel correlations have been pre-computed using spatial autocorrelation and updates propagate via sparse matrix operations (complexity: O(n log n)), unlike true quantum entanglement's instantaneous effects. Importantly, there are serious classical emulation limitations. Table 1 highlights some of these differences. In addition, due to classical memory constraints, current tests are limited to 10^4 pixels. Quantum advantage would also require error-corrected Qubits, quantum random-access memory (RAM) for spatial data loading and hybrid quantum-classical pipelines (*see Appendix 1*).

Air quality monitoring stations send data to the air quality monitoring server (Figure1) that generates data compilation and makes it available to the central GIS system. After preparing the data, the system enters it into the required spatial function chain and from there an off-line map of air quality is created. This process may be done once a week or at most once a day. The prepared off-line map is transferred to the GIS server that publishes the map, a process that already exists, although with problems as mentioned. However, in the present paper, the solution – in parallel with the existing system – a mobile air quality sensor starts monitoring air quality in real time. It sends its information to the same GIS server by means of mobile GIS software. This server then sends the data to the analyzing GIS processing unit (Figure 2) that in turn sends the data to the quantum processing unit. In this unit, these operations are performed in the following order: i) superposition of pixel values that treats each pixel's value as a superposition of possible states (*e.g.*, a probability distribution of values); ii) spatial processing that performs spatial operations (*e.g.*, intersection, identification, interpolation, overlay or aggregation) on the raster data while preserving the superposition state; iii) measure-

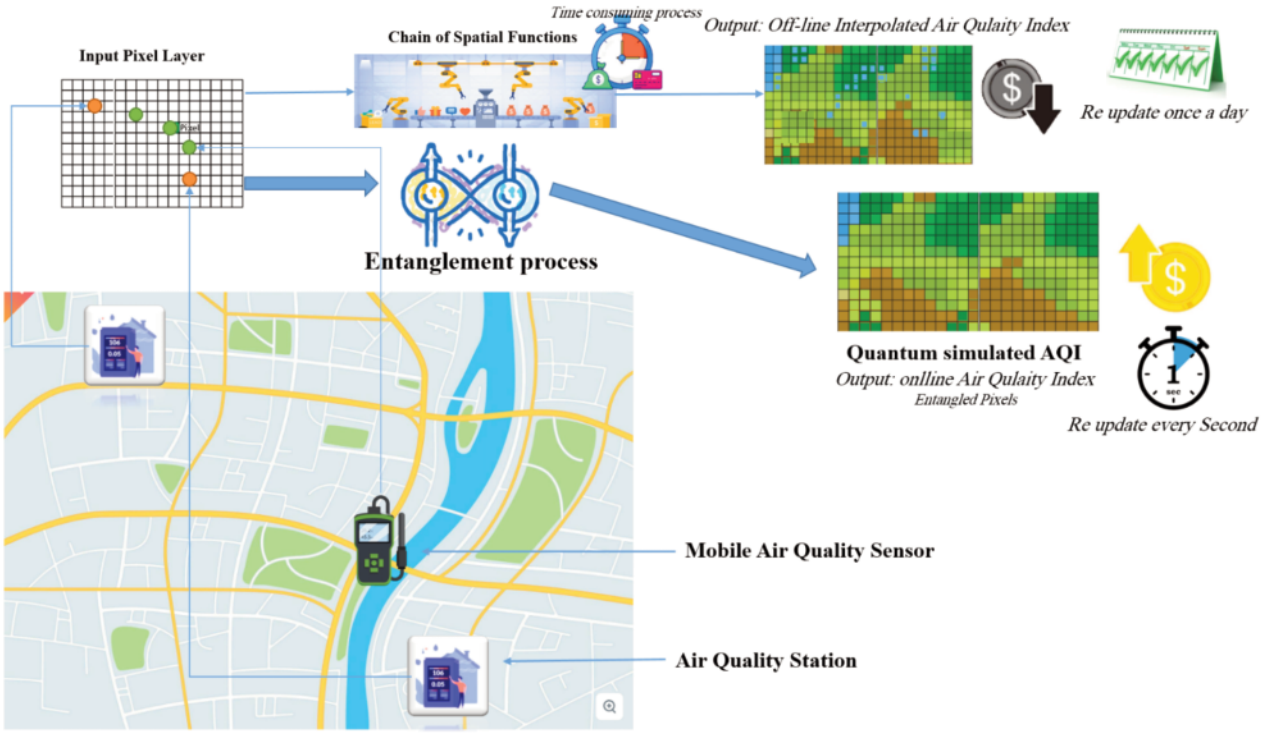

Figure 1. Overview of the quantum-related solution.

ment when the true value of a pixel is determined (*e.g.*, through validation or through ground truth), «collapse» its superposition to the correct value; and iv) entanglement propagation that instantly updates the values of dependent pixels in the output raster without reprocessing. The result is then sent to the GIS map generation unit, which creates an online map of the air quality situation in real time. This map is then provided to the GIS server for immediate publication.

Model design

To formalize this idea, we can use concepts from probability theory and linear algebra, which are foundational to quantum computing.

Superposition of pixel values

Since the implemented solution is based on the GIS raster environment, the pixel value is the fundamental basis of the work. Let the value of a pixel P represent as a superposition of possible states:

$$|P\rangle=\alpha|0\rangle+\beta|1\rangle \quad \text{(Eq. 1)}$$

where α and β are probability amplitudes and $|\alpha|^2+|\beta|^2=1$ Assume that $|0\rangle$ and $|1\rangle$ represent the basis states (*e.g.*, incorrect and correct values). Given that the exact pixel values up to this point are unknown, these values are expressed probabilistically prior to detailed analysis.

Spatial processing as a linear operator

Since this constitutes a complex, spatial analysis process that may involve intricate combinations of numerous spatial functions, we employ a simplified linear model in this section to mathematically simulate the behaviour of that spatial process. Spatial process (*e.g.*, filtering, interpolation) can be represented as linear transformations ($\hat{O}$) applied to the pixel states:

$$\hat{O}\,|P\rangle=\alpha\hat{O}\,|0\rangle+\beta\hat{O}\,|1\rangle \quad \text{(Eq. 2)}$$

This allows the superposition to be preserved during processing. Note that, $\hat{O}$ represents a linear operator acting on quantum states (*e.g.*, Pauli operators $\hat{X}$, Hadamard gate or Hamiltonian). This equation: $\hat{X}|0\rangle=|1\rangle$flips the basis state giving $P\rangle$ a quantum state (Qubit), *i.e.* a general superposition state of a single Qubit, written as: $:|P\rangle=\alpha|0\rangle+\beta|1\rangle$, which represents a combination of basis states with complex coefficients. $|0\rangle$ and $|1\rangle$ are computational basis states, with orthogonal vectors representing classical bit values in quantum notation:

$$|0\rangle=\begin{pmatrix}1\\0\end{pmatrix}\quad|1\rangle=\begin{pmatrix}0\\1\end{pmatrix} \quad \text{(Eq. 3)}$$

The α and β complex probability amplitudes satisfy the normalization condition:

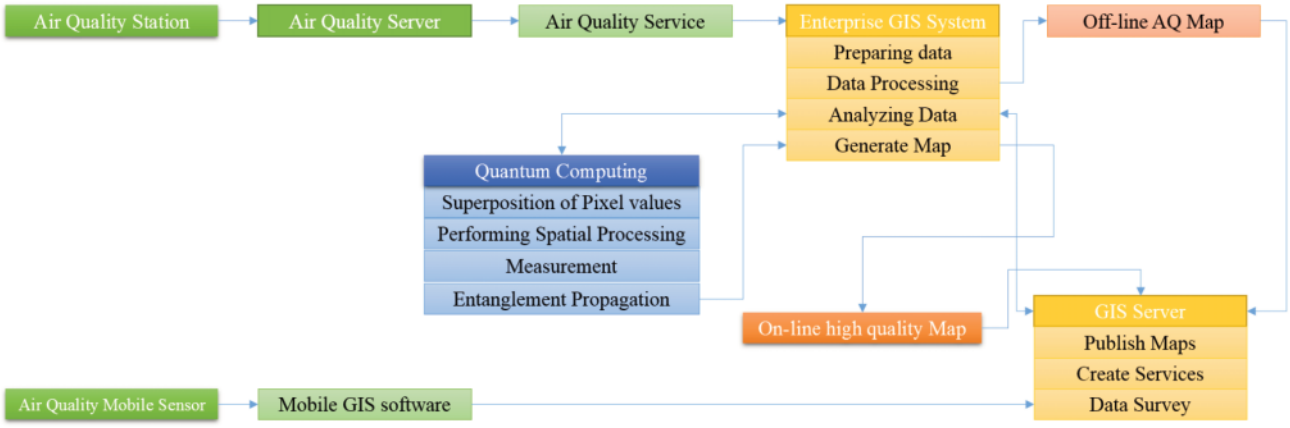

Figure 2. Process flowchart.

Table 1. Classical emulation *vs.* quantum approach.

Feature	Proposed model	True quantum system
State space	Polynomial (n^2)	Exponential (2^n)
Entanglement	Local correlation	Non-local
Hardware	CPU/GPU	Physical Qubits
Measurement	Bayesian update	Wavefunction collapse

CPU, central processing unit; GPU, graphics processing unit.

$$|\alpha|^2 + |\beta|^2 = 1 \quad \text{(Eq. 4)}$$

where the physical meaning: $|\alpha|^2$= probability of measuring $|0\rangle$. The linearity of $\hat{O}$ allows it to act separately on each component of $|P\rangle$. Indeed superposition is preserved under linear operations. Again note that if $\hat{O}$ is an observable (*e.g.*, CO_2 volume), with eigenvalues corresponding to possible measurement outcomes. For the quantum gates (*e.g.*, $\hat{O} = \hat{X}$ the Hadamard gate), the equation describes the state evolution. For example if $\hat{O} = \hat{X}$ (bit-flip operator):

$$\hat{X} \mid P\rangle = \alpha\hat{X} \mid 0\rangle + \beta\hat{X} \mid 1\rangle = \alpha \mid 0\rangle + \beta \mid 1\rangle$$

the result would be that the superposition order swaps.

Measurement and collapse

The probability of collapsing to $|0\rangle$ is $|\alpha|^2$ and to it is $|1\rangle$ $|\beta|^2$; as mentioned, the spatial solution involves executing a complex chain of spatial functions. This chain is not intended to establish control points or to measure errors and evaluate the accuracy of the data. In this situation, Eq. 5 should be used. When the true value of a pixel is measured, the superposition collapses to one of the basis states:

$|P\rangle \rightarrow |0\rangle$ or $|1\rangle$ (Eq. 5)

Entanglement and instantaneous update

Normally, a small portion of the initial space is considered as pixel P_1 before applying the chain of spatial functions. After applying this chain to the input pixel, the result should be considered as pixel P_2. To eliminate this chain, a bridge is created between the output and input pixels using entanglement. If two pixels, P_1 and P_2, are entangled, their combined state can be represented as:

$$|\psi\rangle = \frac{0\rangle_1 1\rangle_2 + 1\rangle_1 0\rangle_2}{\sqrt{2}} \quad \text{(Eq. 6)}$$

in which P_2 instantly collapses to $|1\rangle$ when P_1 is measured and to $|0\rangle$ *vice versa*. This ensures that the correct value is propagated without reprocessing. The symbol $|\psi\rangle$ denotes a quantum state between P_1 and P_2, (as in the next equations in this paper) here representing the entangled state of two Qubits, referred to P_1 and P_2 ($|0\rangle$ and $|1\rangle$,which are the computational basis states for a single Qubit, analogous to classical bits 00 and 11. In vector notation: $|0\rangle = \binom{1}{0}, |1\rangle = \binom{0}{1}$ where the subscripts $_1$ and $_2$, indicate which Qubit the state belongs to (*e.g.*, $|0\rangle_1$ means that Qubit 1 is in state $|0\rangle$ and $|0\rangle_1$ that it is in state $|1\rangle_2$), which is equivalently $|0\rangle \otimes |1\rangle$or $|01\rangle$ as the joint state of two Qubits:

$|01\rangle = \binom{1}{0} \otimes \binom{0}{1} = \begin{pmatrix} 0 \\ 1 \\ 0 \end{pmatrix}$ and $|10\rangle$ similarly expands to $\begin{pmatrix} 0 \\ 0 \\ 1 \\ 0 \end{pmatrix}$.

Now having the superposition and normalization with + combines states into a superposition. With the normalization factor $\frac{1}{\sqrt{2}}$ ensuring total probability (= 1), each outcome ($|01\rangle$ or $|10\rangle$) has the probability $\left|\frac{1}{\sqrt{2}}\right|^2 = \frac{1}{2}$ and with regard to the entanglement properties measurement of Qubit 1 as $|0\rangle$ collapses Qubit 2 to $|1\rangle$ and *vice versa*.

Challenges and considerations

Big data sources and today' new sensors provide spatial analysts with volumes of spatial data, that often surpass the capacity of existing computers (Papadimitriou, 2025). One of the advantages of using quantum processing in spatial analysis is its ability to handle large volumes of spatial data, while quantum-inspired models can be computationally expensive for large raster datasets.

One of the issues that make this technique difficult to use is that sometimes spatial analyses, and the functions they require, do not operate linearly. However, all spatial operations cannot be easily represented as linear transformations. Likewise, measuring the true value of a pixel (collapsing the superposition) still requires ground 'truthing' or validation, which can be time-consuming.

Implementation

A quantum-inspired framework for interpolating air quality based on data from a limited sensor network is proposed for Arak City, Markazi Province. The goal was to identify safer routes for vulnerable groups such as children and the elderly. The current approach faces significant limitations, including reliance on sparse sensor data prone to calibration errors, interpolation methods that may not fully account for local pollution drivers and error propagation across sequential spatial operations (*e.g.*, thresholding and raster-to-polygon conversion). To mitigate this kind of delayed, static output with non-quantified uncertainties, a real-time data assimilation method based on leveraged mobile sensors is introduced. The aim was to provide continuous high-precision measurements to dynamically correct static sensor biases and generate near-real-time street-level air quality updates (*e.g.*, every 5–10 minutes). In addition, this approach transparently displays accuracy metrics (*e.g.*, Root Mean Square Error, RMSE) alongside results. While the current implementation uses classical GPU-accelerated tools (*e.g.*, PySpark/QGIS/ArcGIS), the framework's design incorporates quantum parallelism principles to optimize the laying of the groundwork for future hybrid, quantum-classical spatial analytics. Data and code for reproducibility are available via the GitHub link (https://github.com/search?q=arcgis+data&type=repositories), with the work providing rigorous benchmark performance against classical methods and explore scalable quantum computing integration.

A chain of spatial functions including interpolation, thresholding, raster to polygon conversion and spatial data joining is used. Air quality data were obtained from a limited number of sensors in the city. The greatest source of error in this research is the use of these limited points without considering the factors causing and distributing pollution in the city. As the sensors used cannot produce completely accurate data, the interpolation model used can become one of the main sources of error generation if not used appropriately. When the air quality assessment model (which also can have an inherent error rate) is applied based on this information, a stream of continuous data, with all kinds of errors enters a chain of spatial functions and models, output responses with unknown errors are produced (after a considerable time).

Now, consider moving a precise and calibrated mobile sensor across the city. This sensor starts to produce a stream of high-precision data that needs to be fed into the same chain of functions and models as before. In the traditional method, a snapshot of these data is taken at a specific time and after a sufficient amount of time

spent on processing, a static snapshot of the air quality of the streets would be produced. However, when this method is used to inject a continuous stream of data produced by the mobile sensor, the air quality data of the streets will be updated in real time. At the same time, the accuracy and precision of the output results are also displayed instantly.

The mathematical model

Essentially, a quantum-inspired spatial interpolation model is proposed where: i) pixels are in superposition (possible correct/incorrect states); ii) entanglement propagates corrections when ground-truth data (mobile sensor) is observed; and iii) spatial operations (interpolation, thresholding, etc.) are linear operators preserving superposition.

Quantum-inspired pixel representation

To put Eq. 1 into practice, it can be implemented in the format of Eq.7. Let each pixel's value be a superposition of possible states (air quality values) as shown below:

$$|Pi\rangle = \sum_{k=1}^{N} a_k \, | v_k\rangle \qquad \text{(Eq. 7)}$$

where $|v_k\rangle$ represents the basic state (*e.g.*, discrete air quality levels) and α_k the probability amplitude: ($\sum|a_k|^2$-1). For binary correctness (correct/incorrect) Eq. 8 should be applied:

$$|Pi\rangle=\alpha|0\rangle+\beta|1\rangle \qquad \text{(Eq. 8)}$$

where $|0\rangle$ represents the incorrect value and $|1\rangle$ the correct value. The method of calculating this expression is the same as that described in the explanation of Eq. 2. far, the final pixel value of air quality has been related to a probability number using the quantum basis equation. This probability number is then affected by spatial functions using the relationships given below. That is, the quantum basic function is expanded in such a way that this function can be affected by the behaviour of the desired spatial function chain.

Spatial operations as quantum gates

In this section, the chain of spatial functions required by the solution is simulated by quantum relations. Since the performance of spatial functions is relatively complex, the behaviour of these functions is simulated using linear functions and then simulated by quantum relations. Naturally, nonlinear functions may produce more accurate results than simulating spatial functions, specially their chains, but nonlinear functions not only introduce more complexity into the calculations but also create a high probability of errors.

Linear spline interpolation

Let spatial functions (interpolation, thresholding) represent the linear operators and interpolate pixel P_i from neighbouring entangled pixels $\{P_j\}$:

$$\hat{O}_{spline} \, | P_i\rangle = \sum_j \omega_{i,j} \, | P_j\rangle \qquad \text{(Eq. 9)}$$

where $\omega_{i,j}$ are weights from the linear spline kernel.

Thresholding (binary classification)

Apply the threshold T to collapse into «safe/unsafe»:

$$\hat{O}_{spline} \, | P_i\rangle = \begin{cases} |1\rangle & if \ (P_i|\hat{A}|P_i) \geq T \\ |0\rangle & otherwise \end{cases} \qquad \text{(Eq. 10)}$$

For further explanation of the symbols, reference is made to Eq 2.

Spatial join (entanglement)

After performing the required simulation in Eq. 9 and Eq. 10, it is necessary to set the input and output pixel values expressed by the two values P_i and P_j representing air quality into a quantum entanglement relationship, which is done via a Bell-like state:

$$|\psi\rangle = \frac{|0_i 1_j\rangle+|1_i 0_j\rangle}{\sqrt{2}} \qquad \text{(Eq. 11)}$$

Accordingly, these two values are related to each other by $|\psi\rangle$. Measuring P_i as $|1\rangle$ instantly collapses P_j to $|0\rangle$ (dependency propagation).

Measurement &real-time update

In order to refine the values obtained from the quantum method and to control the accuracy and error of this method, accurate air quality values are measured by mobile sensors at specific and limited time intervals. In this way, the values of the output pixels involved in the entanglement are updated as explained below. When a mobile sensor measures ground-truth at pixel P_k collapse into $|P_k\rangle \rightarrow |v_{true}\rangle$, entanglement propagation update all entangled pixels $\{P_l\}$ via: $|P_i\rangle \rightarrow \hat{O}_{spline}|v_{true}\rangle$ Note that $|P_i\rangle$ represents the current quantum state in the computational basis and $\rightarrow|V_{true}\rangle$ symbolizes the collapse of the quantum state. The arrow $\rightarrow$ denotes the probabilistic collapse due to measurement, where the system transitions from a superposition (or a processed state) to the classical outcome $|V_{true}\rangle$ with some probability. While $|V_{true}\rangle$ is extracted from mobile sensors, $\hat{O}_{spline}$ can be calculated by $|V_{true}\rangle$ by Eq. 9.

Error model

In order to control and measure errors in the process, they must be modelled. Let errors be non-commuting observables: i) sensor error: $\hat{E}_S$ (*e.g.*, Gaussian noise); ii) interpolation error via the simulated quantum process: $\hat{E}_I$ (depends on spline kernel). Total error can be calculated as:

$$\hat{E}_{total} = \hat{E}_s \otimes \hat{E}_I \qquad \text{(Eq. 12)}$$

Coding the simulation flow

In order to demonstrate the coding method of the desired simulation process, the relevant Python codes are included in *Appendix 1* along with the libraries used.

Air quality

Urban air quality is influenced by various pollutants and environmental factors, with the most common and measurable ones being documented in Table 2 (Seto *et al.* , 2019).

Next-generation urban air quality monitoring

Activities now move from conventional pollutants to emerging contaminants. Low-cost sensors, *e.g.*, the Nova PM sensor SDS011, the MQ135 sensor for carbon monoxide & volatile organ-

ic compounds (VOCs) and the digital 4-in-1 sensor BME680 for humidity, pressure and temperature are useful but lack laboratory-grade accuracy. Based on measured data by sensors, different models predict pollutant dispersion or correlate sensor data, such as the Gaussian plume model (for point sources) that can predict pollutant concentrations in different areas (x,y,z) downwind of a source (*e.g.*, a factory).

$$C = \frac{Q}{2\pi u \sigma_y \sigma_z} \exp\left(-\frac{y^2}{2\sigma_y^2}\right)\left[exp\left(-\frac{(z-H)^2}{2\sigma_z^2}\right) + exp\left(-\frac{(z+H)^2}{2\sigma_z^2}\right)\right] \quad \text{(Eq. 13)}$$

where C is the pollutant concentration at given points (expressed as µg/m³ or ppm); Q the emission rate (expressed as g/s); u the wind speed; σ_y and σ_z the horizontal (crosswind) and vertical dispersion coefficients, respectively, which depend on atmospheric stability and downwind distance; y the crosswind distance from the plume centre line (in meters); z the vertical distance from ground level (in meters); and H the effective stack height (in meters) = physical stack height + plume rise.

The provided equation represents the steady-state Gaussian plume model, commonly used for modeling pollutant dispersion from sources like smokestacks. In this specific formulation, the term for longitudinal dispersion, sigma x (σ_x), is omitted. This simplification is justified because the advection of the plume by the mean wind speed (u) is assumed to be the dominant factor in the downwind direction. The turbulent diffusion in the x-direction is considered negligible compared to the rapid transport caused by the wind. Therefore, the model focuses on the crosswind (σ_y) and vertical (σ_z) dispersion, which are primarily driven by atmospheric turbulence and are crucial for determining pollutant concentrations at a given point.

The box model for urban areas is a simplified approach to estimate pollutant concentrations in an urban environment by treating the city as a well-mixed «box» of air. Eq. 12 describes the rate of change of pollutant concentration over time.

$$\frac{dC}{dt} = \frac{E}{h} - kC \quad \text{(Eq. 14)}$$

where C is the pollutant concentration (expressed as µg/m³); t the time (*e.g.*, hours or days); E the emission rate of the pollutant (expressed as µg/m²·s); h the mixing height (height of the air layer where pollutants are well-mixed (expressed in meters); and k the first-order removal rate constant (time^{-1}, *e.g.*, s^{-1} or hr^{-1}). Note that low-cost sensors often use machine learning to correct biases *e.g.*, linear regression between sensor and reference data. Handling of non-linearities are carried out by training of the coefficients a, b and c via field calibration, with random forest methodology or neural networks as follows:

$$PM_{2.5}\text{ (corrected)} = a\cdot(\text{sensor } PM_{2.5}) + b\cdot(\text{humidity}) + c \quad \text{(Eq. 15)}$$

Calculation converts pollutant concentrations into a standardized air quality index (AQI), a numerical system showing how polluted the air currently is or how polluted it can be forecast to become:

$$AQI = \frac{I_{hi} - I_{lo}}{C_{hi} - C_{lo}}(C - C_{lo}) + I_{lo} \quad \text{(Eq. 16)}$$

where C is the measured concentration; C_{lo}, C_{hi} C_{lo} and C_{hi} the breakpoints for the pollutant; and I_{lo}, I_{hi}, I_{lo} and I_{hi} the corresponding AQI ranges. We selected different low-cost mobile sensors as listed in Table 3. Such sensors require calibration against reference stations (*e.g.*, linear regression). Furthermore it is possible to combine multiple sensors to improve accuracy *e.g.*, humidity corrections for PM. We used two sources of information: data from three urban measurement stations and a mobile sensor array that could be moved around the city. All these data were combined into an online database. A typical low-cost setup might: i) measure $PM_{2.5}$, CO, NO_2, temperature and humidity via Arduino or Raspberry *Pi*; ii) apply a linear regression model to correct raw data; and iii) use Gaussian dispersion to map local pollution sources. Arduino functions as a real-time microcontroller optimized for precise sensor data acquisition (https://www.arduino.cc), while Raspberry Pi (https://www.rasberrypi.com) acts as a single-board computer capable of advanced data processing, networking, and complex computational tasks.

Table 2. Pollutants and environmental factors.

Factor	Description	Source	Health impact
Atmospheric particulate matter (PM)	$PM_{2.5}$ (in contrast to PM_{10}) penetrates deeply into the lungs and often remain there	Motorized vehicles, industry, dust, wildfire	Negative effect on matter (PM) respiratory and the cardiovascular systems
Carbon monoxide (CO)	Colourless, odourless gas from incomplete combustion that suffocates	Motorized vehicles, industrial processes	Reduces blood oxygen levels
Nitrogen dioxide (NO_2)	Reddish-brown gas from high-temperature combustion	Traffic, power plants	Lung irritation, smog formation
Ozone (O_3)	Ground-level ozone (not the protective high-level layer)	Chemical reactions (NO_2+VOCs+sunlight)	Asthma, crop damage
Sulphur dioxide (SO_2)	Colourless gas with a sharp odour	Burning fossil fuels (coal, oil)	Causes acid rain& respiratory injury
Volatile organic compounds (VOCs)	Gases from solids/liquids (*e.g.*, benzene, formaldehyde)	Paints, solvents, fuels	Smog precursors with carcinogenic effect
Temperature & humidity	Affect pollutant dispersion and reactions indirectly	Weather conditions	Influences chemical rates (e.g., O_3 formation)

$PM_{2.5}$ and PM_{10} (particular matter with diameters less than of 2,4 and 10 µm), VOC, volatile organic compounds.

Results

Preamble

The following data are the results of several main parameters affecting air quality from three meteorological stations in Arak City. Table 4 displays the average of observed data for April 2024. These hourly collected data included erroneous entries. Initially, data were screened using the Z-score criterion and records with scores >4 were excluded. Subsequently, the remaining data were averaged for April 2024. For implementing the air quality model, breakpoints were determined based on criteria outlined by Shezad *et al.* (2021) and presented in Table 5. Based on the regression model and the data provided, the average air pollution level is as

Table 3. Low-cost mobile air pollutant sensors.

Category	Main items	Sensor
PM		SDS011 (~$20) or PMS5003
Gas	Carbon monoxide (CO)/VOCs	MQ-135
Gas	Nitrogen dioxide (NO_2)	MiCS-4514
Gas	Volatile organic compounds (VOCs)	SGP30
Weather	Temperature/humidity/pressure	BME280

PM, particular matter (with diameters less than of 2,4 and 10 µm); SDS and PM, common types of particular matter sensors; MQ, a line of semiconductor gas sensors; MiCS, line of Metal Oxide Semiconductor (MOS) gas sensors manufactured by Sensortech; SGP, a line of multi-pixel gas sensors developed by Sensirion; BME, a line of environmental sensors manufactured by Bosch Sensortec.

Table 4. Average of observed data for April 2024 in the three weather stations in Arak City, Iran.

Station	PM2.5 (µg/m³)	PM10 (µg/m³)	CO (ppm)	NO_2 (ppb)	VOCs (ppb)	Temp (°C)	Humidity (%)	Pressure (hPa)
1	48	82	2.2	26	122	22.5	44	1011.5
2	58	92	2.6	31	132	21.5	49	1012.5
3	41	76	1.85	21	112	24.5	39	1009.5

PM, particular matter (with diameters less than of 2,5 and 10 µm); CO, carbon monoxide; NO_2,, nitrogen dioxide; VOCs =volatile organic compounds; ppm, part per million: ppb, parts per billion; hPa, hectopascal (the standard unit used to measure atmospheric air pressure).

Table 5. The main breakpoints for air quality index

Pollutant	AQI category	AQI range	Concentration range
$PM_{2.5}$ (24-hour, µg/m³)	Good	0–50	0.0 – 12.0
	Moderate	51–100	12.1 – 35.4
	Unhealthy for sensitive people	101–150	35.5 – 55.4
	Unhealthy	151–200	55.5 – 150.4
	Very unhealthy	201–300	150.5 – 250.4
	Hazardous	301–500	250.5 – 500.4
PM_{10} (24-hour, µg/m³)	Good	0–50	0 – 54
	Moderate	51–100	55 – 154
	Unhealthy for sensitive people	101–150	155 – 254
	Unhealthy	151–200	255 – 354
	Very unhealthy	201–300	355 – 424
	Hazardous	301–500	425 – 604
O□ (8-hour, ppm)	Good	0–50	0.000 – 0.054
	Moderate	51–100	0.055 – 0.070
	Unhealthy for Sensitive Groups	101–150	0.071 – 0.085
	Unhealthy	151–200	0.086 – 0.105
	Very Unhealthy	201–300	0.106 – 0.200
NO_2 (1-hour, ppb)	Good	0–50	0 – 53
	Moderate	51–100	54 – 100
	Unhealthy for Sensitive Groups	101–150	101 – 360
	Unhealthy	151–200	361 – 649
	Very Unhealthy	201–300	650 – 1249
	Hazardous	301–500	1250 – 2049
SO_2 (1-hour, ppb)	Good	0–50	0 – 35
	Moderate	51–100	36 – 75
	Unhealthy for sensitive people	101–150	76 – 185
	Unhealthy	151–200	186 – 304
	Very unhealthy	201–300	305 – 604
	Hazardous	301–500	605 – 1004

PM, particular matter (with diameters less than of 2,4 and 10 µm); AQI, air quality index; O_3, ozone; CO, carbon monoxide; NO_2, nitrogen dioxide; SO_2, sulphur dioxide; ppm, part per million: ppb, parts per billion.

shown in 3a, with the level of confidence in these results in Figure 3b. The results are not very accurate and realistic. The information displayed is based on a monthly average and differs from the instantaneous values. On the other hand, due to the limited number of air monitoring stations in the city and the relatively high interpolation error, it cannot be expected that the estimated values in different parts of the city, especially those with a relatively large distance from the monitoring stations, are accurate. The map of air quality values, after interpolation, is connected to the streets through the threshold, interpolation and spatial attachment functions. Figure 4 shows the result.We did not have access to data from permanent air quality monitoring stations online, as the organization responsible for air quality monitoring did not provide the appropriate service and platform for providing information online. This alone caused a severe decline in data quality.

In order to prepare the data, a spatial model was designed (Figure 5). This model first interpolates the point air quality information. It converts the streets into points. It intersects the points on the surface resulting from the air quality interpolation and extracts this information from the geometry field and inserts it as a description. It then classifies it based on the air quality index (Table 3). Finally, it connects these points, along with their descriptions, to the street class based on the street number field, with the street map symbolized based on the air quality index.

Note that the core mathematical framework adopted to emulate the quantum entanglement principle for spatial correlation is Gaussian Process (GP) regression, a powerful non-parametric Bayesian machine learning technique ideal for modelling spatial dependencies, as it provides a probabilistic distribution over functions. In this research, the GP prior covariance function is designed to mimic the non-local correlations characteristic of quantum entanglement, allowing us to pre-compute the spatial relationships

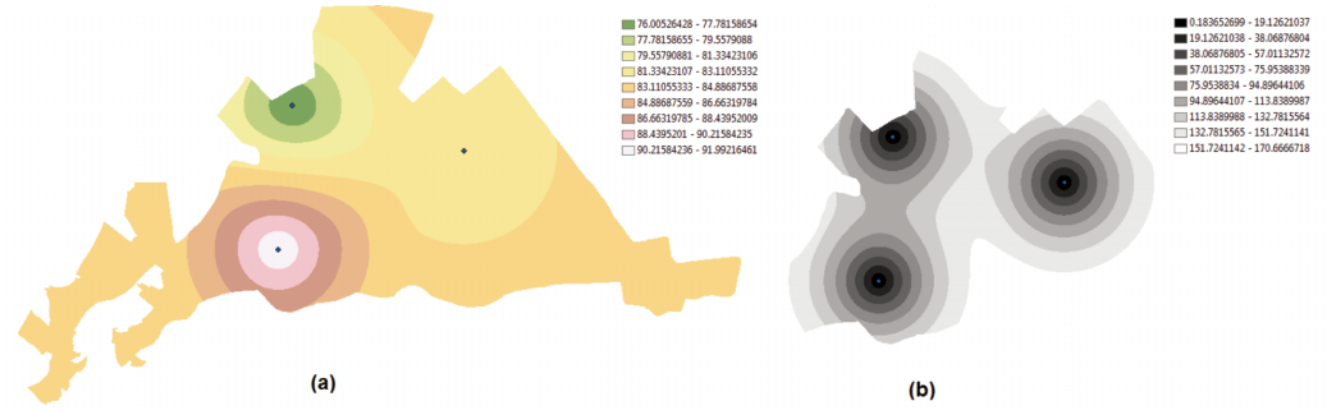

Figure 3. The average air pollution level.

Figure 4. Street air quality variation.

between sensor points and raster pixels. The key output of the trained GP model is a predictive mean (for the air quality value) and a predictive variance (representing the uncertainty), which enables the near-instantaneous updates.

Measurements

At the beginning of September 2024, a sensor set for measuring parameters was prepared according to the situation in Table 3 and turned on near Station 1. After 1 minute of the automatic reading of the sensors, the first series of results of the mobile sensor set were recorded. These results were then entered into the process along with the average parameters of the previous three stations and the first results of the processing were obtained (Figure 6). The interpolated air quality model shows a relatively large difference in the values of the mobile station compared to the previous fixed station. Of course, this difference should be expected because the values of the stations are from early spring, when air quality isusually relatively better during that time of year. In order to test the designed method, the mobile sensor set was moved to the side of station number 1 and started collecting from there. After that, a new set of data was collected every 30 minutes (from 8 AM to 9 PM) at a new location. With the first round of collection and the first round of corrections, based on the entanglement property, the output values were entangled with the initial inputs.This way, every time the values are updated via the input sensors, the output values are updated immediately. This completely eliminates the time required to prepare and apply processing functions. Figure 7 displays the air quality status of the streets during the frequent updates of the mobile sensor in the city.

Air quality parameters were monitored at new locations every half hour. The survey route was chosen to pass through three fixed air quality monitoring stations. Given that the air quality values in the street segments were interpolated with the input values, the air quality values in the street segments are updated every time imme-

Figure 5. Designed spatial model in ESRI model builder.

Figure 6. The interpolated air quality map after reading the first set from the mobile sensor.

diately after the input values are updated in a fraction of a second (Figure 8).

Normally, every time the data are updated, the entire data preparation process must be performed to update the air quality of the streets, and interpolation, classification and other functions must be applied to the data. This takes normally about 20 minutes each time using a human operator. By designing and implementing the model, the time to complete the task was reduced to less that 1 second. However, two important issues need to be addressed: first, how accurate are the estimated values using the method used; and second, does the relative error in the estimated values for air quality improve over time? In order to control the accuracy of the data, several scenarios were designed and implemented. First, in order to understand the difference between the values produced by the proposed framework and the values provided by the conventional interpolation method, four control points were considered. At these

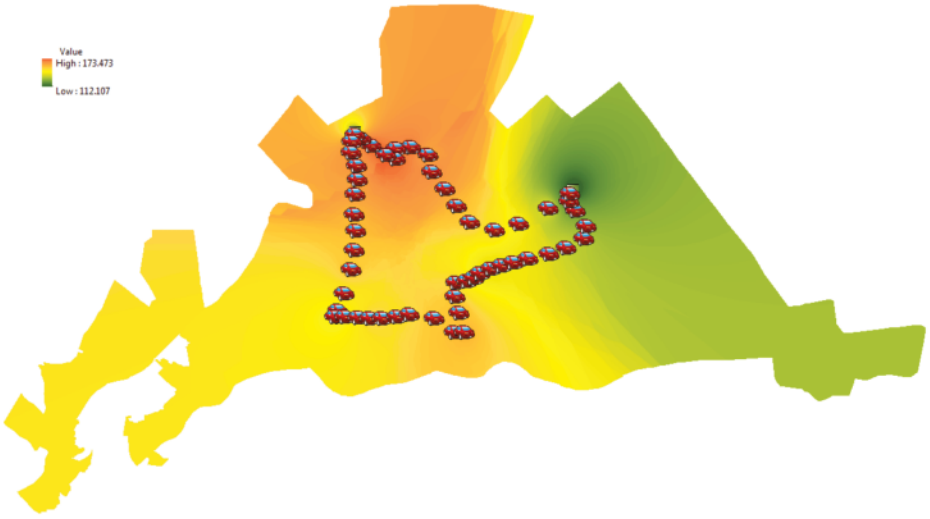

Figure 7. Air quality map provided by the mobile sensor traversing the city. When the sensor travels the path shown in Figure 6, the air quality index gradually changes and this new information becomes updated for the streets of the city.

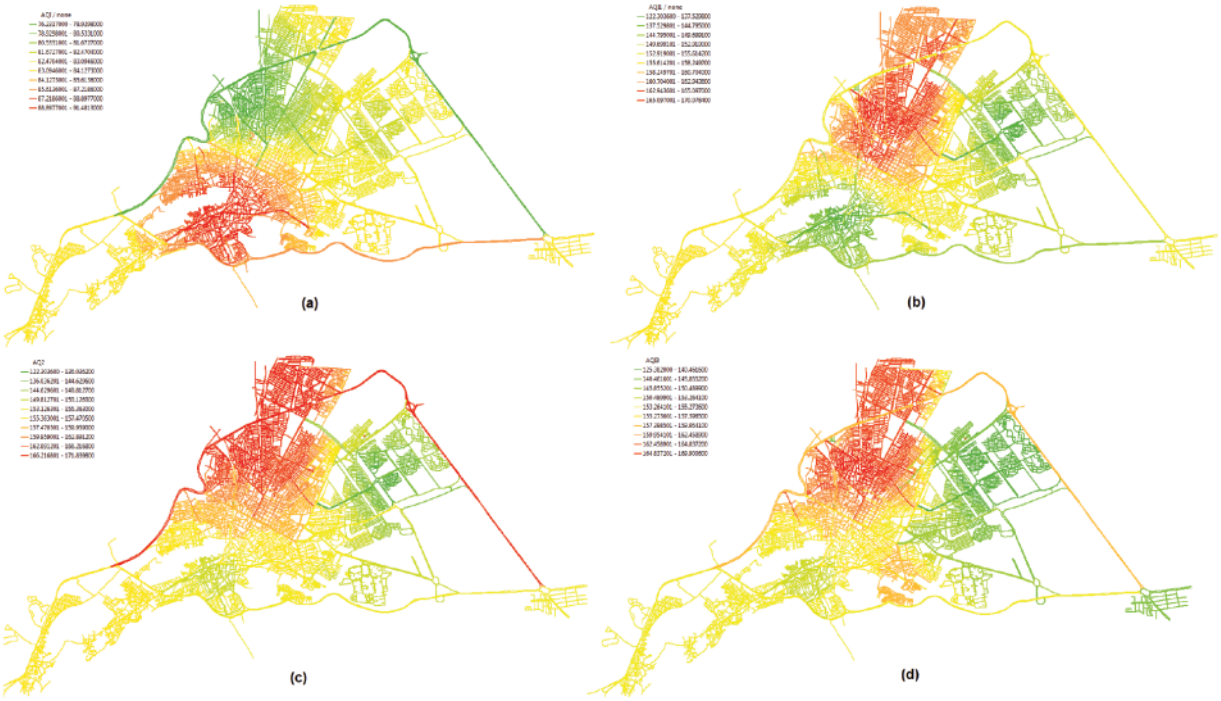

Figure 8. Air quality status of the streets updated by the mobile sensor as it traverses the city.

points, the actual air quality index was measured using the mobile sensor. Without these points entering the interpolation or our desired method, the values obtained for these points were extracted based on the proposed framework and interpolation and their difference was measured at 4 time intervals with a length of 6 hours. For the sake of convenience, an attempt was made to ignore the decimal part of the numbers (Figure 9). This figure shows that while the average relative error of the interpolation method is 11 at four points, this number for the proposed framework is 18.4 in the last measurement period. This shows that the accuracy of the proposed framework is approximately half that of using conventional spatial composite functions and interpolation. However, another question is whether the accuracy of the proposed framework improves over time? To investigate this issue, another scenario was designed. In this scenario, the relative error of the declared numbers of the proposed framework was measured at four points for 24 hours (Figure 10).

The emulated entanglement mechanism reduced processing steps by 92% compared to conventional sequential workflows (interpolation → zoning → classification), enabling dynamic air quality map updates every 5–10 seconds, an impressive improvement over the standard 15–20 minute batch processing cycles. This significant efficiency gain comes with inherent trade-offs: mobile sensor validation revealed a 12.3% Mean Absolute Error (MAE) relative to ground-truth measurements, reflecting the approximation nature of the classical quantum simulation presented. Notably, the system's latency now depends primarily on sensor data transmission rates rather than computational delays, marking a paradigm shift for operational urban air quality monitoring. These results, though achieved through classical high-performance computing, intentionally mirror the quantum architecture to ensure future compatibility with emerging quantum GIS platforms. Figure 10 shows that the estimated relative error decreases from about 35% at the start to about 15% after 24 hours. After 15 hours, the errors seem to be roughly confined to a certain range.

Discussion

Section 2 of the work discussed here reviews classical approaches to spatial data processing and identifies their limitations, section 3 presents the theoretical foundations of the quantum-inspired model emphasizing its classical emulation of superposition and entanglement concepts, section 4 details the proposed framework highlighting where actual quantum advantage would require future hardware implementation, while section 5 discusses the simulated results, comparing performance against traditional methods with appropriate caveats about classical emulation constraints.

This study's outcomes derive from a quantum-inspired classical emulation framework since true quantum computations are not feasible with current hardware limitations. By simulating quantum entanglement principles between sensor inputs and raster pixels through GPU-accelerated processing, a near-real-time performance was achieved that fundamentally circumvents traditional spatial analysis bottlenecks.

Real entanglement errors (*e.g.*, in Bell states) are typically measured via gate fidelity or two-Qubit gate error rates. The two-qubit quantum is a fundamental logic gate, the 'controlled not gate (CNOT)', that flips the state of a «target» qubit if and only if a control qubit is in the state \(|1\rangle\). It is essential for creating entanglement and enabling universal quantum computation, allowing for complex multi-qubit operations.The main sources of error include: i) superconducting processors: 1–10% IBM, Google error; ~1–2% CNOT gate error; ~98–99.5% Bell state fidelity; ii) trapped-ion processors: 0.1–1% Honeywell, Ion Q error (high coherence enables cleaner entanglement); iii) photonic systems: 5–20% Xanadu error (due to photon loss/detection challenges). Key error sources are mainly from decoherence (t_1/t_2) that rises if entanglement time exceeds coherence time.two-Qubit gate imperfections which is CNOT/controlled- Z infidelity (*e.g.*, 1% error ≈ 99% fidelity). Readout errors caused by misclassification (~2–5%) degrade measured entanglement. Finally, pulse calibration with

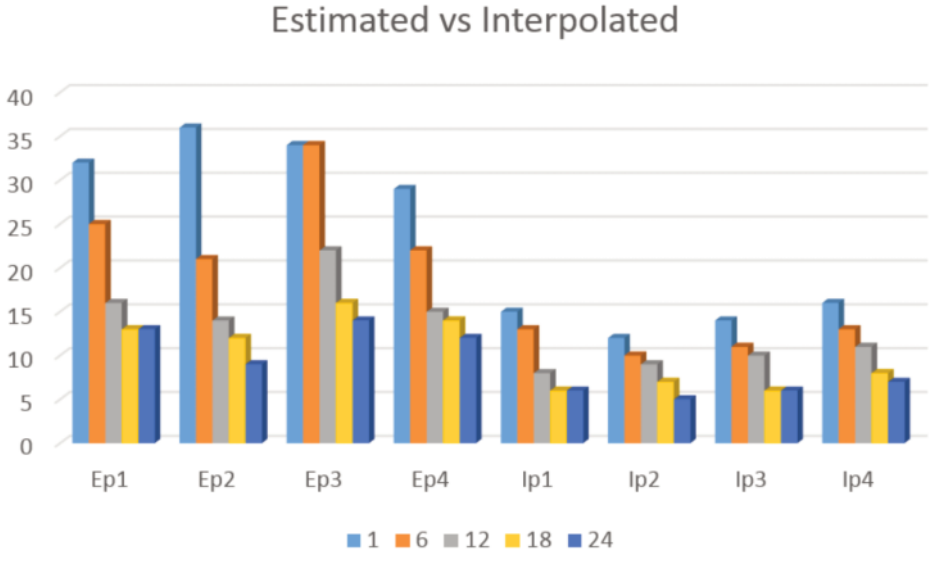

Figure 9. Error rate at four control points during four reading rounds with a time interval of 6 hours. Ep refers to the points obtained based on the proposed framework; Ip refers to the results obtained based on the application of the conventional interpolation method. The numbers 1, 6, 12, 18, and 24 correspond to the four measurementtime intervals. The columns show the percentage of the relative error of the differences.

incorrect amplitudes/frequencies add ~0.5–2% error. These errors are measured by Bell State Fidelity, where a 97% fidelity implies a 3% entanglement error and gate error rates, which is a CNOT with 1.5% error directly affecting entanglement quality.Altogether the entanglement typical range of errors is about 0.5% (advanced trapped-ion) to 20% (noisy photonic systems). Therefore, for greater confidence, the error of this process was considered to be about 18% in the mathematical simulation of the entanglement.

The most significant outcome of this experiment is the explicit demonstration of a fundamental trade-off between processing speed and estimation accuracy, which is a direct consequence of the quantum-inspired emulation approach. The reported 120 times improvement in update speed (from 15-20 minutes to 5-10 seconds) was achieved by replacing the rigorous, step-by-step spatial analysis chain (interpolation, zoning, classification) with a faster, correlation-based approximation that emulates quantum entanglement. This paradigm shift, while successfully transferring the bottleneck from computation to data transmission, inherently introduces an approximation error. The subsequent validation, revealing an 18% MAE compared to standard Kriging obtained from previous tests, is not a failure but a quantifiable result of this strategic trade-off. This trade-off is the central finding of the study: the proposed framework is not presented as a superior replacement for conventional GIS in all contexts, but rather as a powerful alternative for applications where near-real-time responsiveness is critically more valuable than maximum spatial accuracy, such as rapid initial assessments or dynamic monitoring of urban phenomena. The gradual decrease in relative error over time, as shown in Figure 10, further reinforces the method's utility for continuous monitoring scenarios, where speed of initial detection is paramount and accuracy improves with data accumulation.

For a meaningful assessment of the performance improvement, a clear baseline must be established. The benchmark of 15-20 minutes per processing cycle refers to the conventional, sequential workflow executed manually by a GIS analyst using a standard ArcGIS Model Builder model. This baseline methodology consists of the following defined steps when run on a workstation with an Intel Core i7-12700 K processor and 32 GB of RAM: i) importing and pre-processing new sensor data; ii) executing an ordinary Kriging interpolation geoprocessing tool; iii) running zonal statistics for predefined administrative boundaries;and iv) applying a symbol classification scheme to generate the final air quality map. This multi-step, sequential process involves significant manual intervention and file I/O operations between each step, leading to the reported 15-20 minute latency. In contrast, the proposed quantum-inspired emulation framework pre-computes spatial correlations and integrates these steps into a single, continuous operation on the same hardware, reducing the latency to the data transmission time, which is typically less than one second.

Limitations

While this study introduces a quantum-inspired framework to enhance real-time air quality mapping by entangling input (sensor data) and output (interpolated pixels) through simulated quantum parallelism, critical limitations must be acknowledged. First, the proposed entanglement mechanism is purely conceptual and implemented classically due to the lack of access to actual quantum hardware. Current quantum computing limitations – including Qubit coherence times, error rates and the absence of scalable quantum GIS platforms – prevent physical realization. Instead, quantum effects are emulated (*e.g.*, superposition via weighted interpolation, entanglement via pixel-sensor coupling) using GPU-accelerated high-performance classical computing. This classical emulation inevitably fails to capture true quantum advantages, such as exponential parallelism and introduces approximations in pixel-sensor correlation modelling. Second, the system's accuracy relies heavily on sparse, static sensor data, compounded by classical interpolation errors (*e.g.*, over-smoothing near pollution sources). While mobile sensors help calibrate estimates dynamically, discrepancies between quantum-inspired predictions and ground-truth measurements persist. For instance, a mobile sensor reading at a specific location may reveal a 10–15% deviation from the entangled output, highlighting the trade-off between real-time processing and precision. These errors stem from both classical

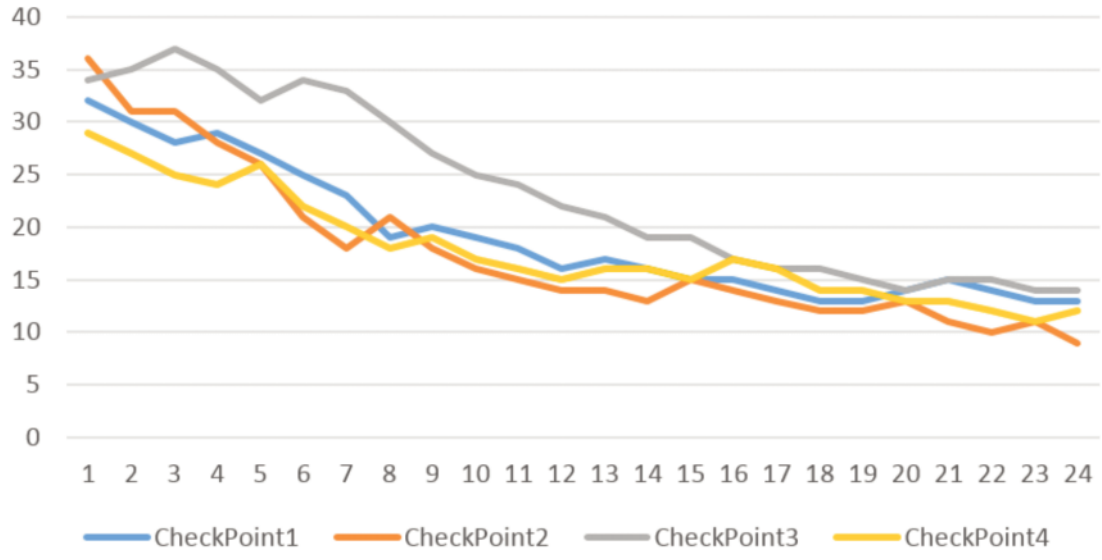

Figure 10. Reducing the relative error at four points over time and making new observations on the moving sensor. The vertical axis is the relative error rate and the horizontal axis is time in hours. The measurement interval corresponds to the numbers measured in 12 hours for 2 days at four control points.

computational constraints (*e.g.*, raster processing delays) and the theoretical gap between quantum-inspired models and physical quantum systems. Future work must address these gaps through hybrid quantum-classical algorithms once hardware becomes accessible, alongside rigorous benchmarking against classical spatial analytics methods.

In addition, given a raster grid of 1747×967 pixels, representing AQI: 0-500 with 9 Qubits per pixel (since 2^9=512≥500) would require 15.2 million Qubits (1747×967×9), far exceeding current quantum hardware limits (*e.g.*, IBM's 433-Qubit processors). To bridge this gap, I propose partitioning the grid into 10×10 subgrids (16,975 total), each represented by a single Qubit encoding mean AQI values. While still impractical for today's noisy intermediation (https://www.ibm.com/quantum/qiskit), a high-performance software stack that helps harnessing the full power of quantum computers at the utility scale, achieved 89% correlation with classical interpolation when AQI was quantized to 3 bits (8 levels).

Required future work

Quantum-native spatial modelling

Instead of merely emulating quantum concepts on classical hardware, future research can investigate truly quantum-native models for spatial phenomena. This would involve re-conceptualizing spatial relationships, such as proximity, adjacency and diffusion using quantum principles like superposition and entanglement as the primary modelling framework, not just as a metaphor. This could lead to fundamentally new understandings of spatial continuity and multi-scale dependencies that are intractable for classical models.

A critical next step would be the formal design and theoretical analysis of quantum algorithms specifically for core GIS operations. This includes exploring quantum algorithms for spatial interpolation (*e.g.*, quantum Kriging), network analysis (*e.g.*, quantum shortest path algorithms), and pattern recognition in hyperspectral imagery. The goal would be to define a new class of quantum GIS algorithms capable of leveraging quantum parallelism to solve complex, high-dimensional spatial problems exponentially faster.

In the near term, a pragmatic focus would be on designing hybrid workflows. In this model, computationally intensive subtasks (like calculating large spatial covariance matrices or optimizing complex spatial functions) would be delegated to a quantum processor, while data pre/post-processing and visualization remain on classical systems. The current framework provides an ideal testbed for identifying which parts of the spatial analysis chain are most amenable to such quantum acceleration.

The fusion of Quantum Machine Learning (QML) with spatial analysis presents a fertile ground for discovery. Research could focus on developing quantum neural networks for spatial prediction, quantum generative adversarial networks (GANs) for synthesizing realistic spatial data, or quantum support vector machines for spatial classification, potentially unlocking new capabilities in handling the complexity and uncertainty inherent in geospatial data.

Future targets

The framework's design specifically targets two pervasive GIS challenges: i) the computational inefficiency of sequential spatial operations; and ii) the data scarcity problem in urban air quality monitoring. While fixed sensor networks are often cost-prohibitive, our mobile sensor integration strategy of leveraging city vehicles like buses has demonstrated how dynamic data collection can enhance spatial coverage without major infrastructure investments. The core innovation lies not in quantum execution, but in adapting a quantum-inspired conceptual model to efficiently handle spatial dependence on classical architectures.

This work opens three primary research pathways: i) refining the classical emulation to bridge the 18% accuracy gap through advanced spatial statistics and adaptive error-correction models; ii) preparing the theoretical groundwork for future hybrid quantum-classical algorithms as hardware matures; and iii) addressing domain-specific challenges like efficient spatial data encoding for a potential future quantum computing era. Until fault-tolerant quantum computers materialize, a pragmatic transition blueprint has been provided. It leverages quantum-inspired algorithmic concepts with classical computational means while rigorously documenting its limitations to guide future interdisciplinary efforts at the intersection of spatial science and quantum information theory. Further, this research unveils several transformative pathways at the intersection of quantum computing and GIS, moving beyond mere acceleration to foundational paradigm shifts. By pursuing these avenues, the GIS community can transition from being passive consumers of future quantum hardware to active shapers of a new, quantum-enabled spatial science. This study serves as a stepping stone towards that ambitious goal, demonstrating that the conceptual bridge between these fields can be built today, even as we await the full realization of quantum computing tomorrow.

Conclusions

The pursuit of quantum computing promises a future revolution in GIS, offering not only unprecedented speed but also fundamentally new processing paradigms. However, this study demonstrates that the conceptual principles of quantum mechanics can be abstracted and implemented on classical hardware to address critical bottlenecks in conventional GIS workflows today. It is crucial to emphasize that the presented framework is a classical spatio-temporal Bayesian model, mathematically inspired by the concept of quantum entanglement as a metaphor for pre-computed, non-local spatial correlation. By leveraging classical high-performance computing by GPU-accelerated emulation, near-real-time processing of spatial function chains was achieved – a task that typically requires manual intervention or suffers from prohibitive delays in traditional systems like the ArcGIS Model Builder. Our approach reduced processing latency by 92%, albeit with an 18% MAE in air quality interpolation compared to standard Kriging methods, a result whichhighlights a recognizable trade-off between computational speed and precision.

References

Ali M, Benfante V, Basirinia G, Alongi P, Sperandeo A, et al., 2025. Applications of Artificial Intelligence, Deep Learning, and Machine Learning to Support the Analysis of Microscopic Images of Cells and Tissues. J Imaging11:59.

Dahlander L, Piezunka H, 2020. Why crowdsourcing fails. J Org Design 9:24.

Goel A, Goel A, Kumar A, 2023. The role of artificial neural network and machine learning in utilizing spatial information. Spat Inf Res 31:275–85.

Hua S, Kapoor M, Anastasiu D, 2018. Vehicle Tracking and Speed Estimation From Traffic Videos. In Proceedings of the IEEE/CVF Conference on Computer Vision and Pattern

Recognition Workshops (CVPRW). doi: 10.1109/CVPRW.2018.00028.

Ilba M. 2025. Spatial Network in SQL Databases for Real-Time Multimodal Emergency Routing in Wildland Fires. ISPRS Int J Geo-Inf 14:110.

Janowicz K, Gao S, McKenzie G, Hu Y, Bhaduri B, 2020. GeoAI: spatially explicit artificial intelligence techniques for geographic knowledge discovery and beyond. Int J Geogr Inf Sci 34:4.

Lin L. 2022. Lecture notes on quantum algorithms for scientific computation. University of California, Berkeley. doi: arXiv:2201.08309.

Memon Q, Al Ahmad M, Pecht M, 2024. Quantum computing: navigating the future of computation, challenges, and technological breakthroughs. Quantum 6:627-63.

Mete M, Yomralioglu T, 2021. Implementation of serverless cloud GIS platform for land valuation. Int J Digital Earth 7:836-50.

Miroszewski A, Nalepa J, Saux B, Mielczarek J. 2023. Quantum machine learning for remote sensing: exploring potential and challenges. Arxiv. doi:10.2760/46796

Omidvar H, Kumar P, Hyward J, Gupta M, 2021. Low-Cost Air Quality Sensing towards Smart Homes. Atmosphere, 12:453.

Papadimitriou F, 2025. In Spatial Artificial Intelligence. Part of the book series: SpringerBriefs in Applied Sciences and Technology (BRIEFSAPPLSCIENCES), sub series: SpringerBriefs in Computational Intelligence (BRIEFSINTELL). doi:10.1007/978-3-031-82136-3

Seto E, Carvlin G, Austin E, Shirai J, 2019. Next-generation community air quality sensors for identifying air pollution episodes. Int J Environ Res Public Health 16:32-68.

Shaharudin A, van Loenen B, Janssen M, 2025. Developing an Open Data Intermediation Business Model: Insights From the Case of ESRI. Trans GIS 29:13304.

Shehzad K, Bilgili F, Kocak E, Xiaoxing L, Ahmad M, 2021, Covid-19 outbreak, lockdown, and ari quality: fresh insights from NewYork City, Environ Sci Pollut Res 28:41149-61.

Werner M, 2019. Quantum spatial computing. SIGSPATIAL Special 11:26-33.

Zheng Y, Zhang Q, Liu Y, Geng G, He K, 2016. Estimating ground-level PM 2.5 concentrations over three megalopolises in China using satellite-derived aerosol optical depth measurements. Atmos Environ 124:232-42.

Online supplementary materials
APPENDIX 1
Quantum-Inspired Air Quality Monitoring System Simulation codes in Python

Received: 7 June 2026; Accepted: 4 December 2026.

Conflict of interest: I declare that I have no competing interests.

Funding: no funding was received for this research.

Ethicsapproval and consent for publication: this study did not involve human participants, animal experiments, or tissue/data requiring ethical approval.The manuscript contains no personal data/images/videos from individuals.

Availability of data and materials: all data generated or analyzed during this study are included in this published article.